



On the crack evolutional in human dentin under uniaxial compression imaged by high resolution tomography

D. Zaytsev ^{1,2}✉, A. Funk ³

¹ Ural State Mining University, Yekaterinburg, Russia.

² Ural Federal University, Yekaterinburg, Russia.

³ Federal Institute for Materials Research and Testing (BAM), Berlin, Germany

✉ dmitry.zaytsev@urfu.ru

Abstract. An observation of the fracture process in front of the crack tip inside a dentin sample by means of ex-situ X-ray computed tomography after uniaxial compression at different deformation values was carried out in this work. This ex-situ approach allowed the microstructure and fracturing process of human dentin to be observed during loading. No cracks are observed up to the middle part of the irreversible deformation in the samples at least visible at 0.4 μm resolution. First cracks appeared before the mechanical stress reached the compression strength. The growth of the cracks is realized by connecting the main cracks with satellite cracks that lie ahead of the main crack tip and parallel its trajectory. When under the stress load the deformation in the sample exceeds the deformation at the compression strength of dentin, an appearance of micro-cracks in front of the main cracks is observed. The micro-cracks are inclined (~60°) to the trajectory of the main cracks. The further growth of the main cracks is not realized due to the junction with the micro-cracks; we assume that the micro-cracks dissipate the energy of the main crack and suppressed its growth. These micro-cracks serve as additional stress accommodations, therefore the samples do not break apart after the compression test, as it is usually observed under bending and tension tests.

Keywords: dentin; crack evolution; compression strength; mechanical properties; microstructure; ex-situ X-ray computed tomography

Acknowledgements. D. Zaytsev is grateful for the financial support of the Russian Science Foundation (RSF project No. 22-29-00268).

Citation: Zaytsev D, Funk A. On the crack evolutional in human dentin under uniaxial compression imaged by high resolution tomography. *Materials Physics and Mechanics*. 2023;51(5): 38-51. DOI: 10.18149/MPM.5152023_5.

Introduction

Human dentin is the hard base of the tooth. It is composed of an organic matrix that is reinforced by carbonated apatite [1]. The main mechanical function of dentin is to distribute mechanical loads within the tooth under mastication. Due to its unique hierarchical microstructure from macroscopic to microscopic length scales, dentin is able to endure both considerable elastic (~ 15 %) and irreversible deformation (~ 15 %) at high strength under uniaxial compression (~ 430 MPa) [2]. On the other hand, its deformation behavior is close to brittle solid under bending and tension. The total deformation of human dentin in three-point bending tests is considerably low (~ 1.5 %) in comparison to uniaxial compression (~ 3 %) [3]. The flexural strength (150-200 MPa) is also lower [3–5]. The ultimate tensile strength of dentin is

40-90 MPa, which is less than the flexural strength and the compression strength [6–8]. This dependence of the strength of dentin samples on the loading scheme is caused by the difference of stress distribution in samples that different mechanisms of deformation and fracture are activated under respective loads under compression, bending, and tension.

It is supposed that the crack growth in dentin is realized due to the junction of the primary or main crack with the secondary or satellite cracks ahead of the main crack tip [9,10]. At that, part of the satellite cracks can nucleate from tiny cracks in the highly mineralized cuff of peritubular dentin [11]. Therefore, the trajectory of the main crack preferably runs through the dentinal tubules [9]. Such a mechanism of crack growth is anticipated for high tensile stresses inside a dentin sample. However, tensile stresses in tensile and three-point bending tests are much higher than in compression tests. Therefore, the fracture process is different under compression test compared to tensile.

It has been shown that the compression strength decreases with an increase of the sample height or, in other words, with decreasing d/h ratio (the ratio between the diagonal d of the compressed sample surface and the sample height h) [2,12]. Samples with a low d/h ratio behave brittle-like while the deformation behavior of samples with a high d/h ratio is close to a ductile. The friction between the sample surfaces and the compression punches under uniaxial compression results in a dependence of the mechanical properties of dentin samples on its d/h ratio. If transverse or tensile deformation is suppressed in region compressed sample surfaces in a sample with a high d/h ratio, an inhomogeneous deformation will occur. As a result, the samples can possess a barrel-like shape after compression [2]. The crack growth in dentin is suppressed when the tensile and the shear stresses are minimized. Indeed, a sample with a high d/h ratio and already present cracks can be compressed several times without any fatal destruction and decreasing the ability to elastic deformation [13]. In this case, intensive deformation should occur ahead of the crack tip. Observations of samples surfaces after compression have shown that the quantity and the length of cracks are decreasing with decreasing of d/h ratio [3]. However, no differences between in profiles of cracks under tension or bending and under compression were observed. The specific reasons for the ability of human dentin to endure significant deformation under compression are still unknown. Is this the result of a decrease in the tensile stresses while compressing or something else? It is possible that the considerable deformation of dentin during compression is caused by the accumulation of micro-cracks in the sample, which do not lead to its destruction due to smaller tensile stresses.

Light microscopy and scanning electron microscopy allow only the sample surface to be observed and provide information about the appearance of cracks on the surface or the fracture surface of a sample. Based on this information, researchers interpret how a crack in the sample can grow. Transmission electron microscopy can estimate the crack growth in the whole volume of a sample but samples for this technique are very thin. Therefore, we obtain two-dimensional information about the crack growth, which is not the case for bulk samples under mechanical testing. However, the assessment of the crack growth within an appropriately large sample volume can be performed using non-destructive three-dimensional imaging techniques such as X-ray computed tomography enables the crack growth to be assessed within an appropriately large sample volume [14,15]. The high-resolution X-ray computed tomography employed in this work (with the resolution up to 0.4 μm) should reveal the relationship between the crack trajectory and the orientation of the dentinal tubules, as the diameter of a single dentin tubular is 1-3 μm [16]. An observation of the crack growth using X-ray computed tomography at different stages of loading will show how cracks nucleate and grow in a dentin sample under compression and may bring new insights as to understand why dentin is able to endure considerable deformation.

Thus, the aim of this work is the observation of the fracture process within dentin samples at different stages of loading by means of high-resolution ex-situ X-ray computed tomography

under uniaxial compression. It is expected that the intensive deformation and fracture processes should occur in front of the main crack tip. The results of this work are potentially useful for the creation of new biomimetic materials, including materials for dental science.

Materials and Methods

Sample preparation. Five intact (caries-free), recently extracted human molars were used in this work. The teeth were obtained from male and female subjects aged 25 to 40 years living within the Ural region (Russia). The tooth extraction procedure was performed according to the Ethical Protocol of the Urals State Medical University in Yekaterinburg that is in accordance with all the requirements of the law. For mechanical testing, from the central part of the teeth crown five cuboid dentin samples were cut out by a diamond saw under continuous irrigation. After that, the surface of the samples was polished by means of the abrasive papers starting with grit 600 and finishing with grit 2000. The samples had a cuboid shape with the approximate size $2 \times 2 \times 0.9 \text{ mm}^3$. The deviation in size was no more than $23 \mu\text{m}$ in height (Z-direction, Fig. 1) and no more than $18 \mu\text{m}$ in the face of the compression plane (X-Y plane, Fig. 1). The measurement accuracy was $5 \mu\text{m}$. The quality of sample surface preparation was controlled using light microscopy (Bresser advance ICD) with the magnification of 50x. There is no strict direction of the dentinal tubules in the samples since they have a large size relative to the tooth where tubules have a complex, sigmoid «S» curvature [14].

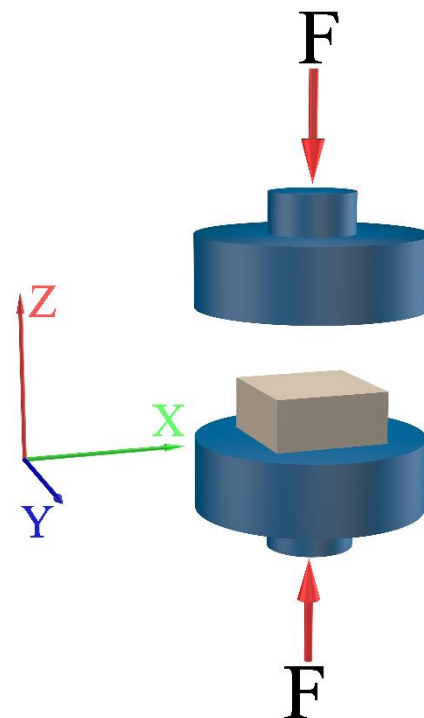


Fig. 1. The scheme of deformation for the dentin samples

Mechanical testing. Until testing the samples were stored in 0.9 % salt solution at ambient temperature before testing. Shimadzu AGX-50kN testing machine has been used for uniaxial compression of the dentin samples. The scheme of loading is given in fig. 1. The tests were carried out with the constant loading rate of 0.1 mm/min. The first sample was not subjected to loading, whereas the other samples 2-5 were loaded up to different deformation values, which are given in Table 1. The deformation values were chosen based on previously performed dentin compression tests, which allow the deformation and fracture process to be estimated during loading from elastic deformation to the start of the fracture process [2].

The deformation of the samples was determined by means of the movement of the traverse. Trapezium-X standard software for Shimadzu was used for processing the experimental data.

Table 1. Dentin sample testing conditions

Sample	Deformation, %	Condition
1	0	initial state
2	7	elastic mode
3	15	irreversible mode
4	25	pre-fracture mode
5	35	after fracture

Microstructure characterization. The observation of the microstructure and the defects within the samples was carried out by means of X-ray computed tomography employing a ZEISS Xradia 620 Versa device. While rotating a sample for 360° within the X-ray beam path, a set of radiographs is captured at discrete angular steps. Subsequently, a three-dimensional volume is reconstructed from the set of radiographs using the standard filtered back-projection algorithm for cone-beam setups [17]. Both data acquisition and reconstruction were performed with ZEISS software "Scout-and-Scan Control" and "Scout-and-Scan Reconstructor" (version 14). Details on the method can be found elsewhere [18].

Overview scans are taken for all five samples at low resolution. Interesting sample spots e.g., ahead of the main crack tips, are tested additionally at high resolution (detail scan). The scanning parameters are summarized in Table 2. Note that besides the voxel size resulting from the total magnification (geometrical and optical), the basic spatial resolution of the device and used objectives is limited. For the high-resolution scans, the total size of the investigated volume was a cylinder with a diameter of 360 µm and a height of 390 µm. ImageJ Fiji, Avizo 2019.4 (ThermoFischer Scientific) and VG Studio max 3.3 (Volume Graphics) were used for image analysis [19–21].

Table 2. Summary of X-ray computed tomography parameters.

	X-ray tube voltage, kV	X-ray tube power, W	Device spec. X-ray filter	Source-Object-Distance, mm	Object-Detector-Distance, mm	Geometrical magnification
Overview scan	50	4.5	LE3	17	17	2x
Detail scan	50	4.5	LE2	11	7	1.633x
	Optical magnification	Total magnification	Voxel size, µm	Basic spatial resolution, µm	Exposure time, sec	Set of radiographs
Overview scan	4x	8x	1.7	1.9	5	801
Detail scan	40x	65.32x	0.4	0.5	30	2401

Results

The deformation stress-strain curves of samples 2-5 under compression are shown in Fig. 2. The trend of deformation curves is similar for all compressed samples. The dependence of the stress on the strain of the samples at the initial stage of loading is linear, while under stress ~ 300 MPa and ~8 % deformation it changes to non-linear. The blue arrows in Fig. 2 points to the stress and the deformation at which the compression test was stopped for each sample.

Sample 2 is compressed to the end of linear deformation (7 %) whereas sample 3 is compressed to the middle part of nonlinear deformation (15 %). The loading of sample 4 was stopped right before the maximum stress or compression strength (25 %) that corresponds to the state of pre-fracture. The deformation under compression of sample 5 was slightly larger than the deformation at which the compression strength was achieved during testing. The gradual stress drop is observed in sample 5 after reaching the compression strength. The stress drop on the deformation curve corresponds to the process of intense fracture or crack nucleation and growth in sample 5.

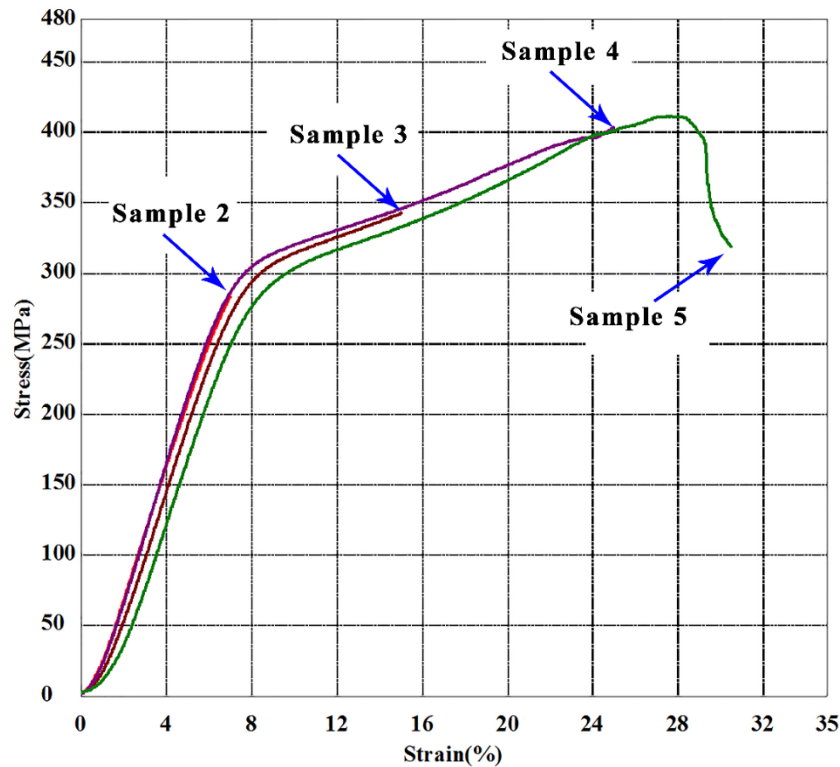


Fig. 2. Deformation curve of dentin sample under compression. Arrows are indicated at the end of the deformation curve for the samples

X-ray computed tomography at low resolution (1.7 μm) of sample 1 and samples 2, 3, 4 and 5 after loading showed that the cracks appear only in samples 4 and 5. The cracks appear at the surface of the samples and penetrate the entire volume. The number of cracks in sample 5 is greater than in sample 4, both on the surface of the sample and inside the sample (Fig. 3). At that, the cracking pattern is similar in both samples. The cracks were almost parallel to the edge of the backside on the compression surface (X-Y plane, Fig. 1) and the cracks are tilted at an angle of 30° to the side surface (Z-Y plane, Fig. 1) for both samples, Fig. 3. In addition, there is a crack in sample 5 (Fig. 5(e)), which is inclined at an angle of 45° to the side surface (X-Y plane, Fig. 1). Besides, there is a secondary crack that begins to grow from the compression surface at the end of the primary crack and it is tilted at an angle of 60° to the side surface of the primary crack (Z-Y plane, Fig. 1) in sample 5. However, despite the similarity of the profiles of the cracks between samples 4 and 5, parallel micro-cracks are observed in the middle part of sample 5 in the area of the main crack tip. The micro-cracks are inclined ($\sim 60^\circ$) to the trajectory of the main crack (Fig. 3(f)). Also, similar micro-cracks are observed directly on the compression surface (X-Y plane, Fig. 1). On the contrary, there are no micro-cracks in the area of the main crack tip in sample 4 (Fig. 3(c)). Both samples 4 and 5 have a barrel-like shape (Fig. 5(c) and 5(f)). Dentin tubules are not viewed at this resolution.

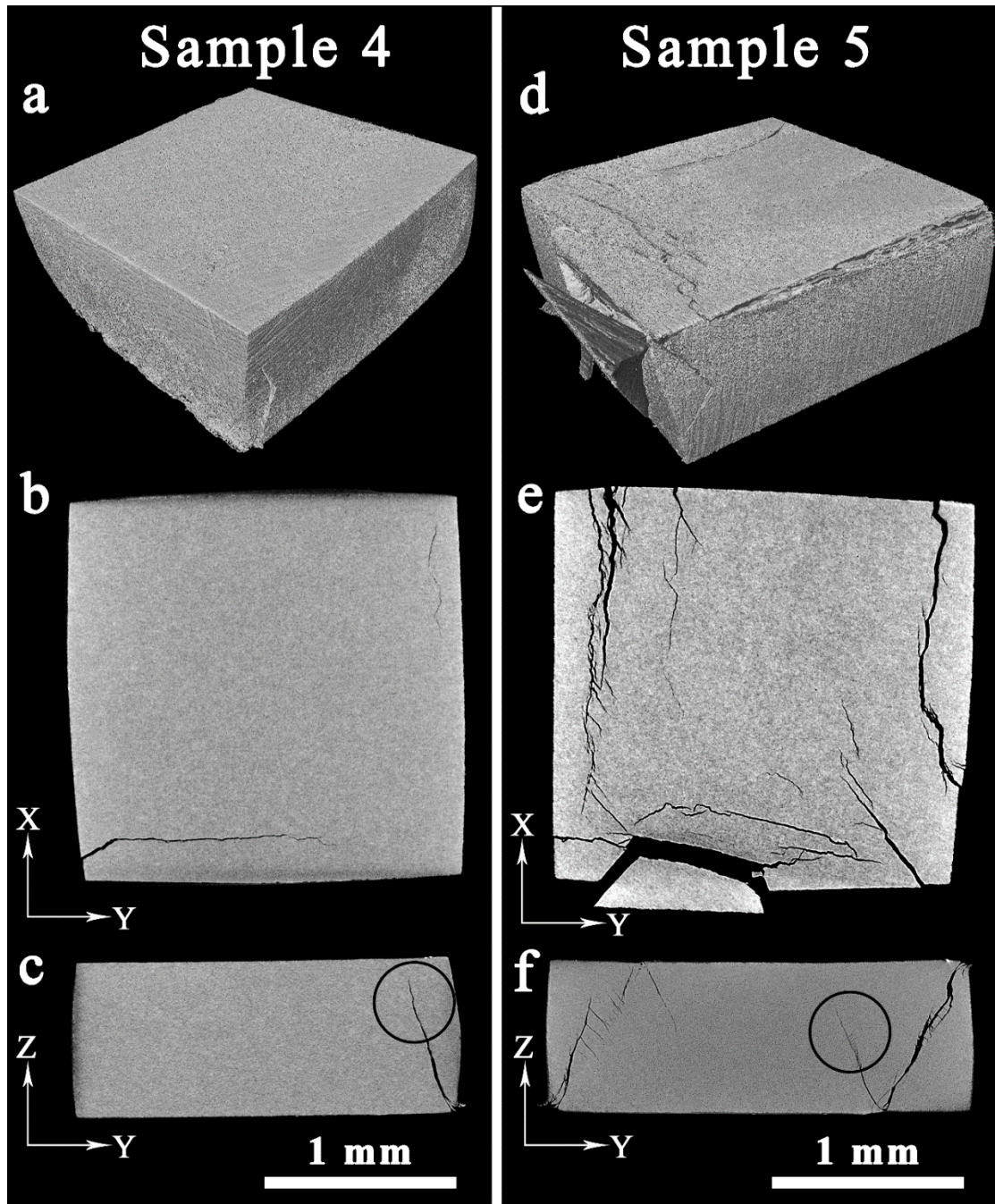


Fig. 3. Overview of the 3D visualization of 4 and 5 samples at low resolution: (a) the view of sample 4; (b) the reconstructed longitudinal slice in the middle part of sample 4; (c) the reconstructed cross-section slice in the middle part of sample 4; (d) the view of sample 5; (e) – the reconstructed longitudinal slice in the middle part of sample 5; (f) the reconstructed cross-section slice in the middle part of sample 5

X-ray computed tomography of samples 4 and 5 after loading at high resolution ($0.4 \mu\text{m}$) was performed in detail for the regions ahead of the main cracks tip (indicated by black circles in Fig. 3(c, f)). The trajectory of the main cracks is uneven, but despite this, the main cracks approximately lie in the planes (Figs. 4(a) and 5(a)). There are satellite cracks lying ahead of the main crack tip for both samples (Figs. 4(b) and 5(b)). The plane of the satellite crack is parallel to the plane of the main crack in sample 4 (Fig. 4(b)). On the contrary, the planes of the satellite cracks are almost perpendicular to the plane of the main crack into sample

5 (Fig. 5(b)). The number of the satellite cracks ahead of the main crack tip is greater in sample 5 (Fig. 5(b)). Dentin tubules are clearly visible at this resolution. Tubules appear as black dots by the overview and as a white line at the view where crack is highlighted (Figs. 4 and 5). In both cases, the trajectory of the main cracks was independent of the alignment of the dentinal tubules.

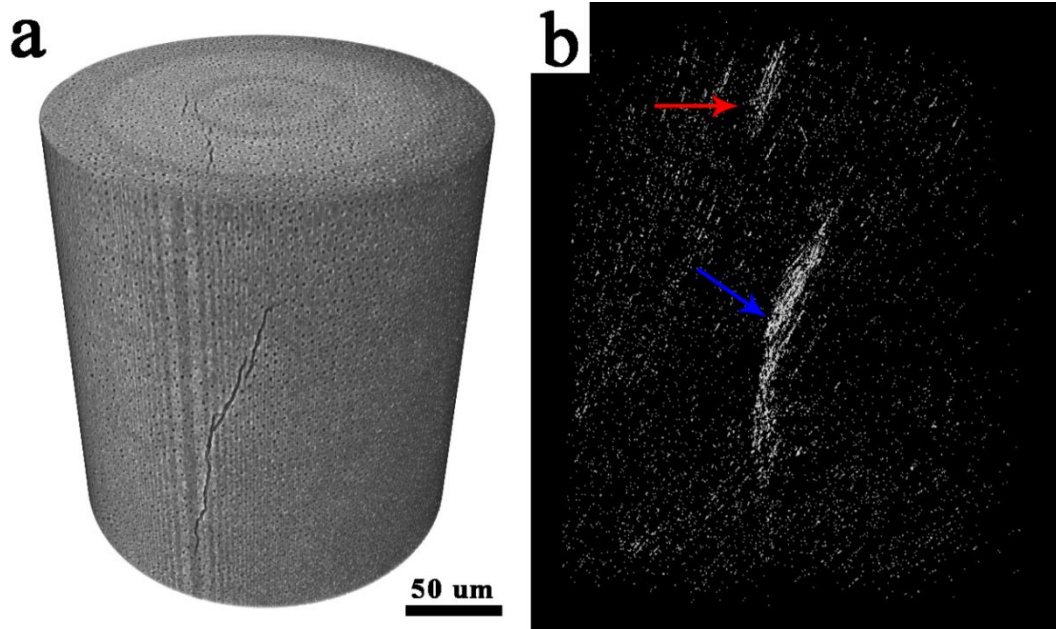


Fig. 4. The 3D visualization of the area of the main crack tip into sample 4 at high resolution (indicated black circle at Fig. 3(c)): (a) the overview; (b) the view where crack is highlighted. The red arrow indicates the satellite crack lying ahead of the main cracks that are indicated by the blue arrow

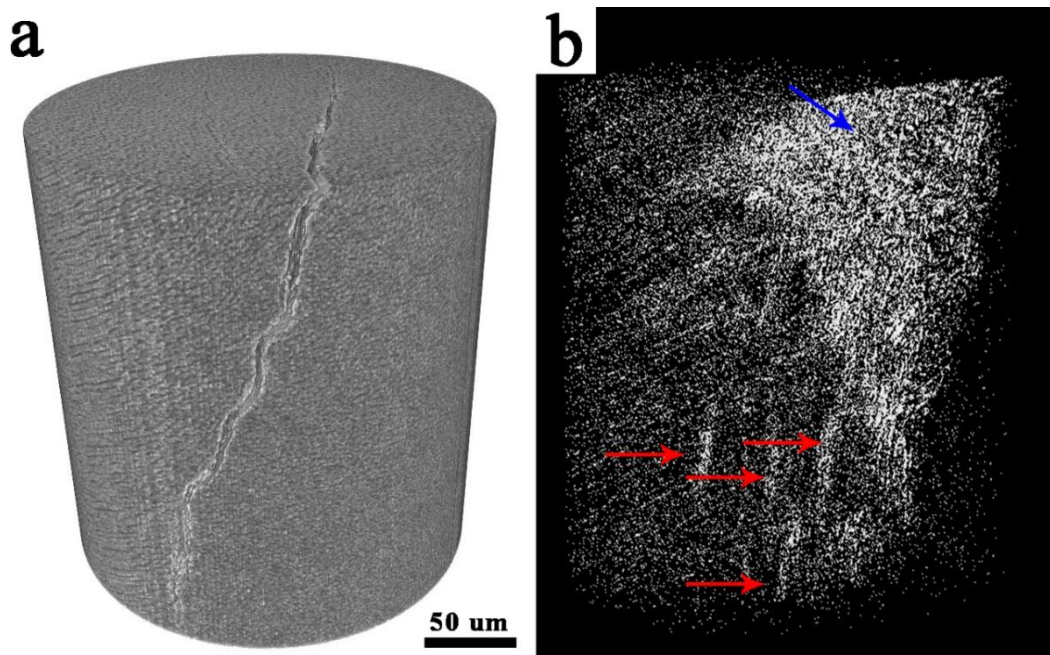


Fig. 5. The 3D visualization of the area of the main crack tip into sample 5 at high resolution (indicated black circle at Fig. 3(f)): (a) the overview; (b) – the view where crack is highlighted. The red arrows indicated the several micro-cracks ahead of the main cracks indicated by the blue arrow

The detailed study of the main crack tip region in sample 4 at high resolution has shown that there are satellite cracks ahead of the main crack tip (Fig. 6). The trajectory of the main crack and the satellite cracks pass through the dentinal tubules (Fig. 6). The trajectory of the main crack and satellite cracks are initially rectilinear but sometimes turn into a zigzag profile (Fig. 6(g)). Besides, tiny cracks inclined ($\sim 60^\circ$) to the main cracks are observed (Fig. 6(h)). The trajectory of the satellite cracks is parallel to the trajectory of the main cracks (Figs. 6(c,e)). At that, not all satellite cracks create a junction with the main crack (Fig. 6(f)). The tiny cracks in sample 5 also branch off from the main crack, but tilted at an angle 30° (Fig. 7(a)). The main crack in sample 5 grows due to the junction with the satellite cracks that lie along further on its growth path as it takes place into sample 4 (Figs. 6(b,c)). However, there are many parallel micro-cracks tilted at an angle 60° to the main crack in sample 5 (Fig. 7). The distance between micro-cracks varies from 16 to $3 \mu\text{m}$. The main crack can pass through micro-cracks, but this does not change its trajectory (Fig. 7(e)). The long micro-cracks have a sigmoid "S" shape profile. Such profile of the long micro-cracks caused by the fact that the cracks started and stopped at the dentinal tubules due to the trajectory of the micro-crack has changed from a straight line to sigmoid "S" near the dentinal tubules (Fig. 7(e)).

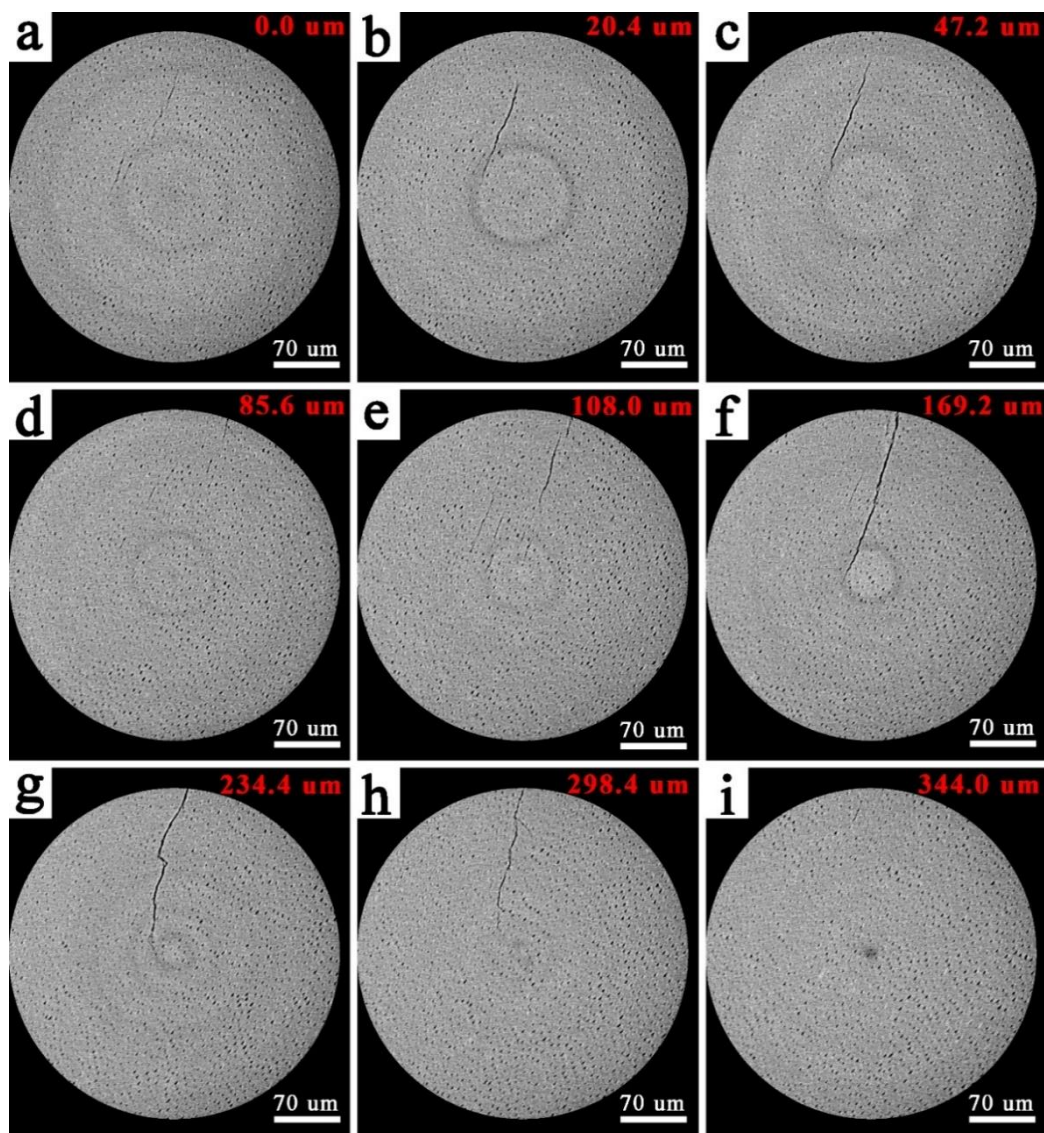


Fig. 6. The reconstructed cross-section slices of the main crack tip area of sample 4 at high resolution (indicated black circle at Fig. 3(c)). Red numbers indicate the layer depth: (a) 0; (b) $20.4 \mu\text{m}$; (c) $47.2 \mu\text{m}$; (d) $85.6 \mu\text{m}$; (e) $108.0 \mu\text{m}$; (f) $169.2 \mu\text{m}$; (g) $234.4 \mu\text{m}$; (h) $298.4 \mu\text{m}$; (i) $344.0 \mu\text{m}$

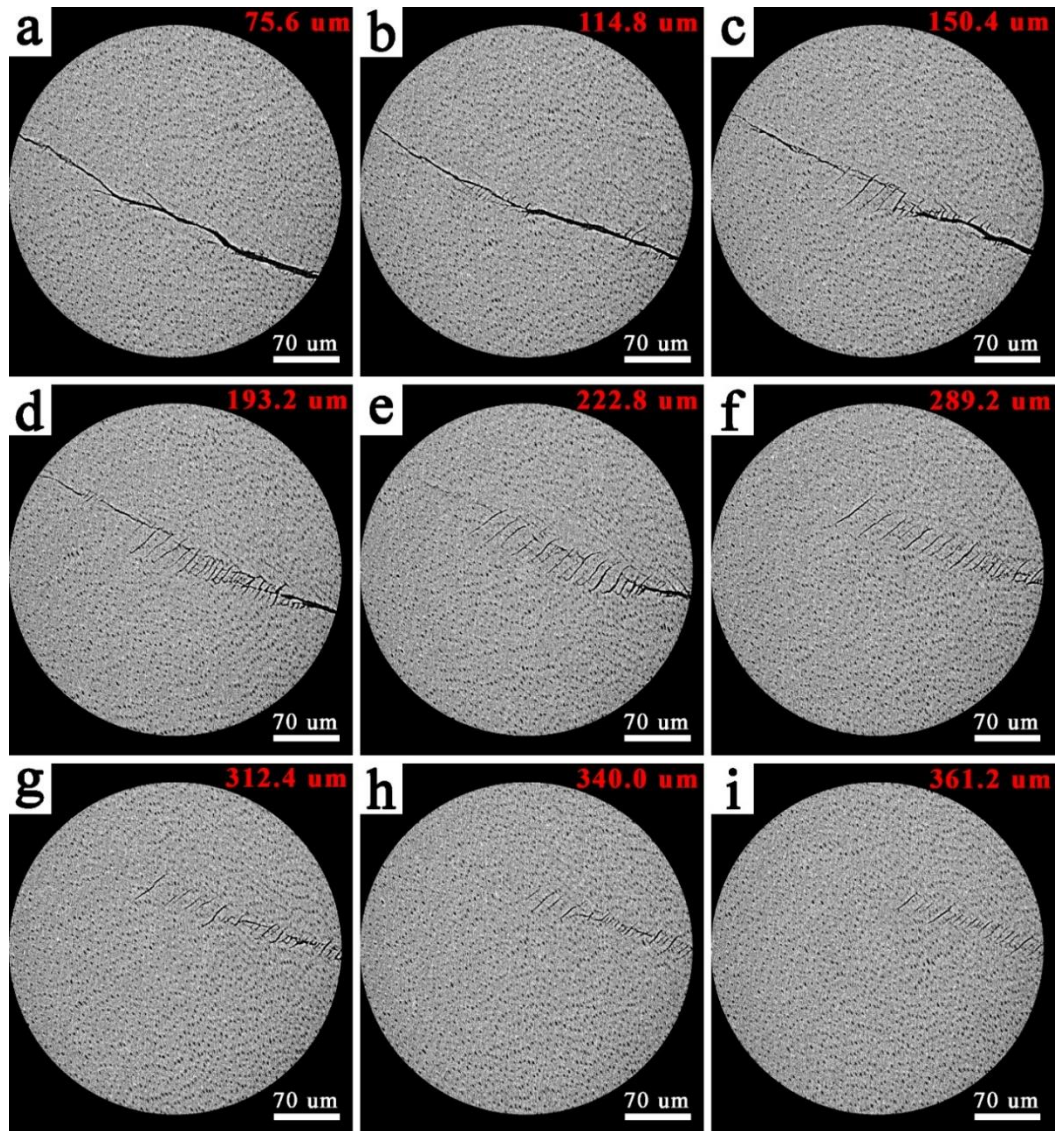


Fig. 7. The reconstructed cross-section slices of the main crack tip area of sample 5 at high resolution (indicated black circle at Fig. 3(f)). Red numbers indicate the layer depth: (a) 75.6 μm ; (b) 114.8 μm ; (c) 150.4 μm ; (d) 193.2 μm ; (e) 222.8 μm ; (f) 289.2 μm ; (g) 312.4 μm ; (h) 340.0 μm ; (i) 361.2 μm

Furthermore, besides the crack pattern, X-ray computed tomography enables studies of the overall microstructure of the samples 1 to 5. A varying number of "pores" was detected at low resolution within the sample series, c.f. (Fig. 8). As the dentinal tubules are not visible at low resolution, the "pores" can be clearly detected without mixing them with the dentinal tubules. The number of individual "pores" in sample 1 is about 900, which is significantly larger than in all other samples; samples 2, 4 and 5 show less than 50 and sample 3 has no more than 5 "pores". In the literature, such "pores" are referred to as "micro-canals" or "giant dentinal tubules" [22]. The "pores" found in the samples 1 to 5 are mostly ranging in size between 6 μm and 20 μm (sphere equivalent diameter) with the mean diameter of about 10 to 12 μm , however, also outliers with about 30 up to 50 μm were found. These outliers are two or more smaller but merged "pores". The detection of "pores" in sample 4 and 5 is challenging due to the dominant crack pattern. The influence of "pores" on the crack evolution is not determined from this sample loading series. Cracks may hit and destroy a "pore" and hence, "pores" will not be

detected anymore. However, "pore" examples were found in sample 5 where the crack avoids hitting the "pores". It is also possible that "pores" will close while compressed. To clarify this, in- or ex-situ X-ray computed tomography from the same sample exposed to loading steps needs to be performed. Nevertheless, X-ray computed tomography proves to be a valuable tool to pre-investigate the quality of tooth samples in advance of any future experimental testing.

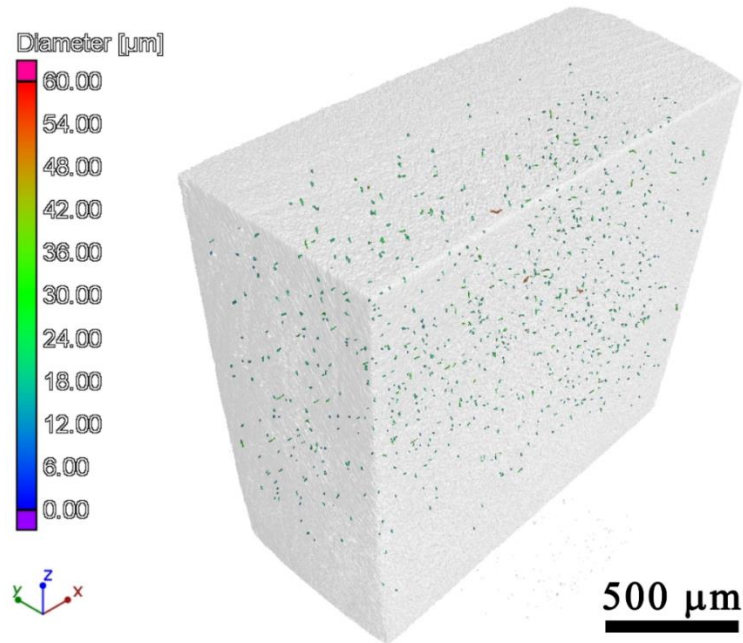


Fig. 8. The 3D visualization of the pore size distribution in sample 1. Color code refers to the pore size equivalent diameter

Discussion

The deformation behavior of compressed dentin samples, when the linear dependence of strain on stress at the initial stage of loading changes to nonlinear at high stresses, is typical for human dentin and elastic-plastic bodies under compression [2]. X-ray computed tomography has shown that the fracture process starts before reaching the compression strength. There are no observed cracks up to the middle of the irreversible deformation of dentin under compression (15 %). Therefore, the considerable elastic and irreversible deformation is not caused by the accumulation of the cracks, at least there is no such evidence at 0.4 μm resolution. Hence, human dentin is able to withstand considerable elastic and irreversible deformation due to its microstructure, but for an implementation it is necessary to create certain conditions. The main one is the reduction of tensile stresses. It was shown by the compression of dentin in liquid nitrogen that the ability to irreversible deformation of dentin is provided by means of the plasticity of collagen fibers and porosity of intertubular dentin [23]. Elastic deformation is realized due to the elasticity of collagen. At high stress loads, when the crack nucleation is starting, intensive deformation occurs in the plastic zone in front of the crack tip. It is clear that highly mineralized cuff withstands less deformation compared to intertubular dentin. During loading and further deformation of dentin, cracking of the peritubular cuff occurs. Since the deformation in the plastic zone is higher than the average deformation for the specimen, the fracture of the peritubular dentin is occurred in front of the tip of the main crack. The tiny cracks nucleate in peritubular cuff [11]. Increasing the deformation leads to an increase in the angle of opening of tiny cracks and their length in peritubular dentin. After that, one of the tiny cracks in the peritubular cuff joint with the tiny crack in the nearest dentin tubular and so on as a result

the satellite crack is formed. Therefore, the crack path lies through the dentinal tubules due to this mechanism of crack growth [9].

The crack growth mechanism under compression is similar to the mechanisms of tensile or bending loadings [10,24]. The main crack grows due to the junction with the satellite cracks that are situated in front of it and lie along its growth path (Fig. 9(a)). However, the micro-cracks are inclined ($\sim 60^\circ$) to the trajectory of the main crack, which was formed when the deformation exceeded deformation at the compression strength (Fig. 7(e)). At that, the growth of the main crack is not taking place due to the junction with the micro-cracks even though the main crack goes through them (Fig. 7(d)). The nucleation of micro-cracks occurs in the plastic zone in front of the tip of the main crack (Fig. 9(b)). This may be due to the accumulated damage in the peritubular dentin in the plastic zone of the main crack that indicates the existence of intense deformation there [25]. The damaged areas of the peritubular dentin are stress concentrators where it is easier for cracks to arise. Similar micro-cracks were observed earlier, where it was defined as "ladder-like" bands that consist of an array of cracks oriented orthogonal to the main band trajectory of the crack [26]. The band texture consists of segments of dentin separated by orthogonal cracks at regular intervals of about $20\ \mu\text{m}$. Shifting and torsion of these segments is thus an energy dissipation mechanism, slowing the crackdown and preventing catastrophic failure [26].

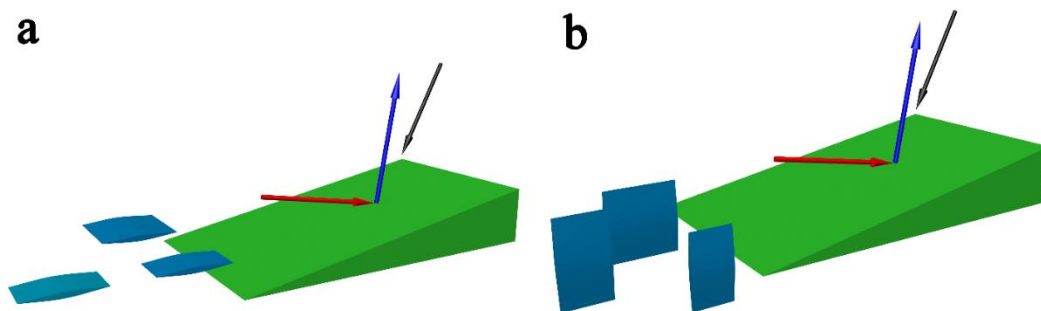


Fig. 9. The schemes of crack grow in human dentin under compression stress: (a) the scheme for crack grows in sample 4; (b) the scheme for crack grows in sample 5. The green wedge is the main crack whereas blue areas are satellite cracks (sample 4) or micro-cracks (sample 5). The red arrows indicated compression stress. The blue arrows indicated tensile stress and the black arrows indicated the direction of dentinal tubules

Stress accommodation of mechanical energy in the sample under the loading is realized due to two channels: deformation and free surface formation (crack nucleation). Deformation of the material in the plastic zone reduces the energy of the crack and can lead to its stop. The nucleation of cracks in front of the main crack tip also decrease its energy. Although the micro-cracks in sample 5 do not join the main crack, micro-cracks are reducing the main crack's energy and suppressing its growth. The micro-cracks act as a shield for the main crack tip and hence, extrinsically toughen the material. Therefore, the nucleation of the micro-cracks is the additional channel of stress accommodation to ligament bridging and crack deviation of the main crack. The samples do not break apart after the compression test due to this channel of stress accommodation as, on the contrary, it takes place under bending and tension. The cracks deviation from the plane of maximum driving force the stress intensity experienced at the crack tip is reduced, thereby providing an additional source of toughening [24]. The formation of a large number of stable cracks in the sample reduces its energy. Due to the sample that contained the cracks can be compressed several times without destruction and decreasing the ability to the elastic deformation [13].

Despite the fact that the crack growth occurs through the dentinal tubules, a strong dependence of the crack trajectory on the orientation of the dentinal tubules was not obtained.

Usually, the relationship between the crack trajectory and the orientation of the dentinal tubules is difficult to evaluate under compression as the orientation, density and diameter of the dentinal tubules in the sample of such volume is nonhomogeneous. There is a significant increase in tubule density and tubule diameter with increasing distance from dentin enamel junction in the tooth [27]. It has been reported that dentinal tubules possess sigmoid "S" shape distribution in coronal dentin [28,29]. Therefore, the dentinal tubules in the samples have different orientations relative to the direction of the compression. Scanning of the areas at the tip of the crack at high resolution showed that the orientation, density and diameter of the dentinal tubules is uniform in a given volume (Figs. 4 and 5). However, in both cases (samples 4 and 5) the angles of inclination of the main cracks and the satellite cracks to the dentinal tubules were different. Therefore, the crack growth trajectory is determined by the scheme of deformation and the shape of the sample, and not by the orientation of the dentinal tubules. On the other hand, the fracture behavior of elephant dentin depends on the orientation of dentinal tubules under indentation where imprint depth was small and comparable to the diameter of dentinal tubules [30]. Besides, the deformation and the fracture behaviors of dentin are anisotropic at some other tests such as shear test, bending and diametric compression [24, 31-33]. It is possible that in those tests the main deformation is realized in a plane whereas under compression the entire sample volume is involved in deformation process under compression.

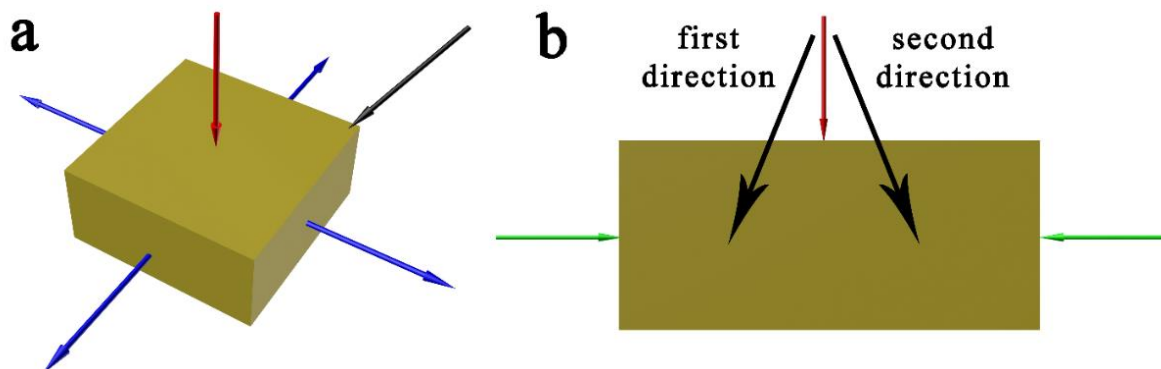


Fig. 10. The schemes forces and stresses acting on the sample under compression: (a) common view of the sample; (b) cross-section of the sample. The red arrows indicated compression stress. The blue arrows indicated tensile stress and the green arrows indicated the direction of the friction forces. The black arrow indicated the direction of dentinal tubules

The reason of the nucleation of the micro-cracks in the plastic zone of the main crack is caused by the scheme of loading and the shape of the sample. Two forces act on the sample when it is compressed: one is directed along the compression axis – the loading force (along Z, Fig. 1), and the second is the friction force between the sample and the compression plate. The friction forces are perpendicular to the compression force and lie in the X-Y plane in Fig. 1 (Fig. 10(a)). Therefore, the vector sum of the loading force and friction forces acts on the sample under compression. The friction forces are directed toward the center of the sample or opposite to tensile stress inasmuch as the sample expands under compression. The friction forces are maximal in the directions of the diagonals of the sample since it has a square cross-section. Two forces act on the sample if we consider the cross-section in the Z-Y Plane (Fig. 1) of the sample (Fig. 10(b)). Indeed, it can be seen that in the cross-section of sample 5, two directions of crack growth are active (Fig. 3(f)). The first direction is inclined at an angle of 30° to the upper compression surface, and the second direction is inclined at an angle of 30° to the lower compression surface (Fig. 3(f)). The cracks grow in the planes of maximum driving forces where tensile stresses are maximal. At that, the crack moves from one surface to another, and the secondary crack begins at the crack exit point on the sample surface (Fig. 3(f)). The micro-

cracks appear in the second direction for a crack moving in the first direction and *vice versa*, a crack moving in the second direction has micro-cracks in the first direction. Hence, the satellite cracks in two directions are formed in the plastic zone in front of the crack tip under the action of two forces where the damaged zone is formed. At low loads, the damaged zone is not large enough for secondary satellite cracks or micro-cracks to nucleate there. There is a damage zone formed inside the plastic zone. The damage zone is situated ahead of the main crack tip and its shape is not circular. The width of the damage zone is $\sim 60 \mu\text{m}$ and its length is $\sim 120 \mu\text{m}$ according to the size of the area of the micro-cracks (Figs. 5(b) and 7(e)). The damage zone can be determined as the pre-fracture zone. Micro-cracks do not nucleate under tension and bending since there is no effect of friction forces.

Conclusion

The considerable elastic and irreversible deformation is not caused by the accumulation of the cracks at least visible at $0.4 \mu\text{m}$ resolution up to the middle of the irreversible deformation of the dentin under compression. The cracks appear right before reaching the compression strength. The mechanism of crack growth under compression is similar to the crack growth under tensile test or three-point bending. The main crack grows due to the junction with the satellite cracks that are situated in front of it and lie along its growth path. However, the micro-cracks that are inclined ($\sim 60^\circ$) to the trajectory of the main crack appear when the deformations exceed the deformation at the compression strength. The growth of the main crack is not realized due to the junction with the micro-cracks. However, it is suggested that the micro-cracks decrease the energy of the main cracks and suppress their growth. These micro-cracks are an additional channel of stress accommodation due to which the samples do not break apart after the compression test as, on the contrary, it takes place under bending and tension.

References

1. Waters NE. Some mechanical and physical properties of teeth. *Symp. Soc. Exp. Biol.* 1980;34: 99–135.
2. Zaytsev D. Correction of some mechanical characteristics of human dentin under compression considering the shape effect. *Mater. Sci. Eng. C.* 2015;49: 101–105.
3. Zaytsev D, Ivashov AS, Mandra JV, Panfilov P. On the deformation behavior of human dentin under compression and bending. *Mater. Sci. Eng. C.* 2014;41: 83–90.
4. Arola DD, Reprogl R. Tubule orientation and the fatigue strength of human dentin. *Biomaterials.* 2006;27: 2131–2140.
5. Staninec M, Nguyen H, Kim P, Marshall GW, Ritchie RO, Marshall SJ. Four-point bending evaluation of dentin-composite interfaces with various stresses. *Med. Oral. Patol. Oral. Cir. Bucal.* 2008;13: 81–84.
6. Giannini M, Soares CJ, Carvalho RM. Ultimate tensile strength of tooth structures. *Dent. Mater.* 2004;20(4): 322–329.
7. Fuentes V, Ceballos L, Osorio R, Toledano M, Carvalho M, Pashley DH. Tensile strength and microhardness of treated human dentin. *Dent. Mater.* 2004;20: 522–529.
8. Nishitani Y, Yoshiyama M, Tay FR, Wadgaonkar B, Waller J, Agee K, Pashley DH. Tensile strength of mineralized/demineralized human normal and carious dentin. *J. Dent. Res.* 2005;84(11): 1075-1078.
9. Yahyazadehfar M, Ivanchik J, Majd H, Zhang BAnD, Arola D. On the mechanics of fatigue and fracture in teeth. *Appl. Mech. Rev.* 2014;66(3): 1–19.
10. Kruzic J, Nalla RK, Kinney JH, Ritchie RO. Mechanistic aspects of in vitro fatigue-crack growth in dentin. *Biomaterials.* 2005;26(10): 1195–1204.
11. Imbeni V, Nalla RK, Bosi C, Kinney JH, Ritchie RO. In vitro fracture toughness of human dentin. *Journal of Biomedical Materials Research Part A.* 2003;66A(1): 1–9.

12. Zaytsev D, Panfilov P. On some features of the shape effect in human dentin under compression. *Mater. Sci. Eng. C*. 2014;45: 205–209.
13. Zaytsev D, Grigoriev S, Panfilov P. Deformation behavior of human dentin under uniaxial compression. *Int. J. Biomater.* 2012;2012: 854539.
14. Kinney JH, Nalla RK, Pople JA, Breunig TM, Ritchie R. Age-related transparent root dentin: mineral concentration, crystallite size, and mechanical properties. *Biomaterials*. 2005;26(16): 3363–3376.
15. Gudkina ZV, Argunova TS, Gutkin MYu. Nondestructive 3D-evaluation of human dentin by microtomography using synchrotron radiation. *J. Phys.: Conf. Ser.* 2019;1410: 012066.
16. Kinney JH, Marshall SJ, Marshall GW. The mechanical properties of human dentin: a critical review and re-evaluation of the dental literature. *Crit. Rev. Oral. Biol. Med.* 2003;14(1): 13–29.
17. Feldkamp LA, Davis LC, Kress JW. Practical cone-beam algorithm. *J. Opt. Soc. Am. A*. 1984;1(6): 1–2.
18. Buzug, TM. *Computed Tomography - From Photon Statistics to Modern Cone-Beam CT*. Berlin; Springer; 2008.
19. *ImageJ wiki software*. Available from: www.imagej.net. (Accessed 14.12.2021)
20. *Thermo Fisher scientific*. Available from: www.thermofisher.com. (Accessed 14.12.2021)
21. *Volume Graphics*. Available from: www.volumegraphics.com. (Accessed 14.12.2021)
22. Sumikawa DA, Marshall GW, Gee L, Marshall SJ. Microstructure of primary tooth dentin. *Pediatr. Dent.* 1999;21(7): 439–444.
23. Zaytsev D, Panfilov P. Influences of the sample shape and compression temperature on the deformation behavior and mechanical properties of human dentin. *Mater. Sci. Eng. C*. 2014;43: 607–613.
24. Nalla RK, Kinney JH, Ritchie RO. Effect of orientation on the in vitro fracture toughness of dentin: the role of toughening mechanisms. *Biomaterials*. 2003;24(22): 3955–3968.
25. Cheboksartseva MA, Zaytsev D, Ivashov AS, Mandra JV, Zholudev S. On the Possibility of Describing the Microstructure of Human Dentin as Soft Matrix Filled by Solid Particles. *J. Phys. Conf. Ser.* 2021;1945: 012057.
26. Fleck C, Burke M, Ganzosch G, Müller C, Currey JD, Zaslansky P. Breaking crown dentine in whole teeth: 3D observations of prevalent fracture patterns following overload. *Bone*. 2020;132: 115178.
27. Montoya C, Arola D, Ossa EA. Time depend deformation behavior of dentin. *Arch. Oral Biol.* 2017;76: 20–29.
28. Nanci A. *Ten cate's oral histology: Development, structure, and function*. 7th ed. St. Louis MO: Mosby; 2008.
29. Zaslansky P, Zabler S, Fratzl P. 3D variations in human crown dentin tubule orientation: A phase-contrast microtomography study. *Dent. Mater.* 2010;26(1): 1–10.
30. Lu X, Fernandez PM, Bradley RS, Rawson SD, O'Brien M, Hornberger B, Leibowitz M, Tozzi G, Withers PJ. Anisotropic crack propagation and deformation in dentin observed by four-dimensional X-ray nano-computed tomography. *Acta Biomaterialia*. 2019;96: 400–411.
31. Watanabe LG, Marshall GW, Marshall SJ. Dentin shear strength: Effects of tubule orientation and intratooth location. *Dent. Mater.* 1996;12(2): 109–115.
32. Zaytsev D, Ivashov AS, Panfilov P. Anisotropy of the mechanical properties of human dentin under shear testing. *Materials Letters*. 2015;138: 219–221.
33. Lertchirakarn V, Palamara JEA, Messer HH. Anisotropy of tensile strength of root dentin. *J. Dent. Res.* 2001;80(2): 453–456.

THE AUTHORS

Zaytsev Dmitry 
e-mail: dmitry.zaytsev@urfu.ru

Alexander Funk 
e-mail: alexander.funk@bam.de